THE BIGGEST, BADDEST, COOLEST STARS
ASP Conference Series, Vol. 412, © 2009
Donald G. Luttermoser, Beverly J. Smith, and Robert E. Stencel, eds.

Of Photons, Gas, and Dust: The Mira Mixmaster

Donald G. Luttermoser
Department of Physics & Astronomy,
East Tennessee State University, Johnson City, TN 37614, USA

Abstract. The physical processes in the atmospheres of asymptotic giant branch (AGB) stars have many important attributes. Their large mass-loss rates impact their evolution and enrich the metal content in the Galaxy. Virtually all AGB stars vary in brightness, which includes the Mira-type variables. The Mira brightness variability is caused by pulsations which produce a 'shocked' atmosphere. Excitation and ionization collisional rates are small in comparison to radiative rates, due to the low densities, which makes the LTE approximation invalid. The cool atmospheric temperatures of these stars allow molecules and dust to form which further complicates the picture – the formation of these species may not be in equilibrium either. Atmospheric modeling of these stars has followed two different approaches: (1) the hydrostatic (HS) method and (2) the hydrodynamic (HD) method. Each of these techniques has its limitations. Dust is often seen in these stars and dust formation is an important component to the chemistry of these atmospheres and to the mass loss. This paper will highlight what has been done to date in modeling the atmospheres of these stars and make suggestions as to what should be done in future modeling attempts.

1. Introduction

Near the end of their thermonuclear lives, low mass stars ($M < 5$-$7\ M_\odot$) cool and expand to very large sizes as they ascend the asymptotic giant branch (AGB). Typically, these stars have a collapsing carbon and oxygen core surrounded by a helium-rich shell that suffers from occasional shell flashes. Meanwhile, the outer layers pulsate as a result of the opacity driven κ-mechanism. This pulsation causes brightness changes that can last from a few months to over a year. As a result of this brightness variability, these stars are referred to as *Long Period Variable* (LPV) stars. If the optical brightness changes by at least 2.5 magnitudes with periods greater than 100 days, the LPV star is called a *Mira Variable* star.

Modeling AGB and red giant branch (RGB) stars has had a long history. Atmospheric modeling of these stars has followed two different approaches: (1) the hydrostatic (HS) method and (2) the hydrodynamic (HD) method. Both of these techniques often employ the following assumptions and approximations: (a) one-dimensional geometry (either assuming a plane-parallel atmosphere or a spherically symmetric atmosphere), (b) chemical homogeneity and equilibrium, (c) dust formation is either ignored or handled in a simple fashion, and (d) magnetic fields are absent or negligible.

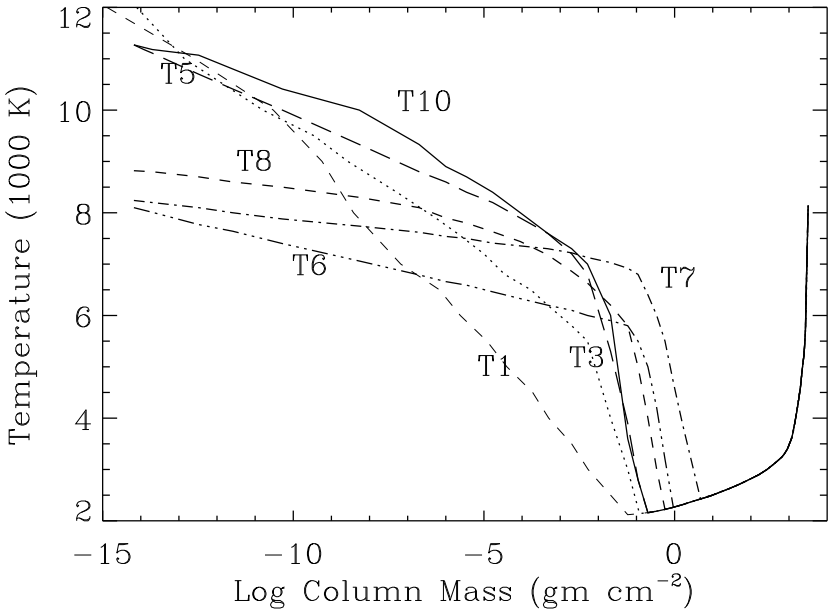

Figure 1. Various semiempirical chromospheric models of the cool semiregular LPV star g Her from Luttermoser et al. (1994).

1.1. Hydrostatic Models

Hydrostatic equilibrium (HSE) is assumed for the pressure as a function of stellar radius. Radiative and convective equilibrium (RE) are often assumed in these models giving temperature as a function of radius — the so-called classical (photospheric) models. A temperature rise can be added to a photospheric model and adjusted until synthetic spectra from the model matches an observed spectrum. This technique is often referred as *semiempirical chromospheric modeling* (see Figures 1 and 2).

1.2. Dynamic Models

In these types of models, the equations of mass, momentum, and energy conservation are solved simultaneously. One solves these equations by either setting up a grid and letting the gas flow past the grid points – the so-called *Lagrangian method*, or one can ride along with the gas – the so-called *Eulerian method*. An example of such models generated with the Lagrangian method can be seen in Figure 3 (Bowen 1988). The dynamic models also can employ the following assumptions: (a) the shocks are isothermal, and (b) shocks are adiabatic. Both of these assumptions however have severe limitations. The isothermal shock assumption will not produce temperature enhancements to form in the shock. Such temperature enhancements are needed to produce emission lines which are seen in the observed spectra of these stars. The adiabatic assumption cannot be valid since heat loss will occur in the shocks due to radiative cooling from the above mentioned emission lines.

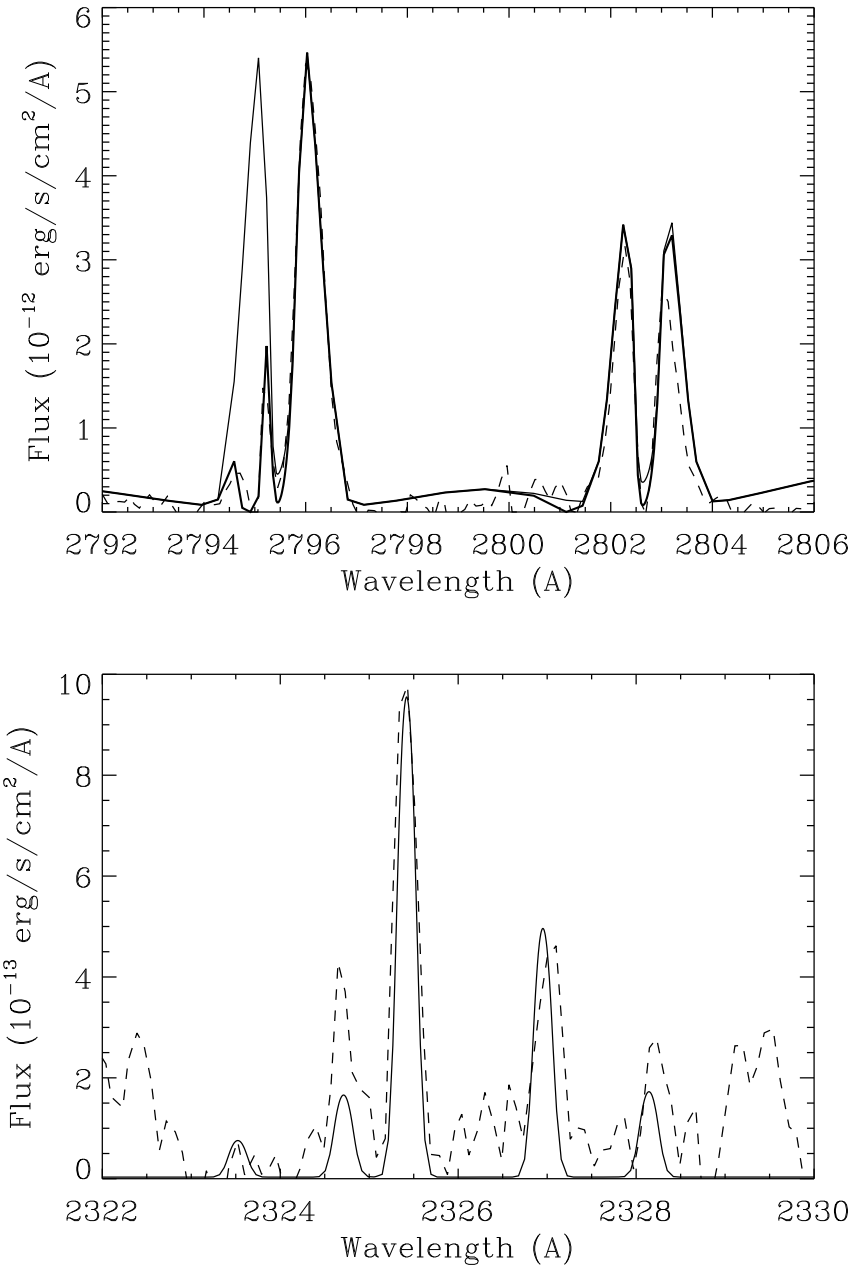

Figure 2. The NLTE Mg II k and h lines synthetic spectrum (*top*) and the NLTE C II (UV0.01) synthetic spectrum (*bottom*) of the T10 model of Figure 1. The synthetic spectra (solid line) are compared to an IUE observed spectrum of g Her. The Mg II spectrum comparison has a third model including a circumstellar shell (thick line). Figures from Luttermoser et al. (1994).

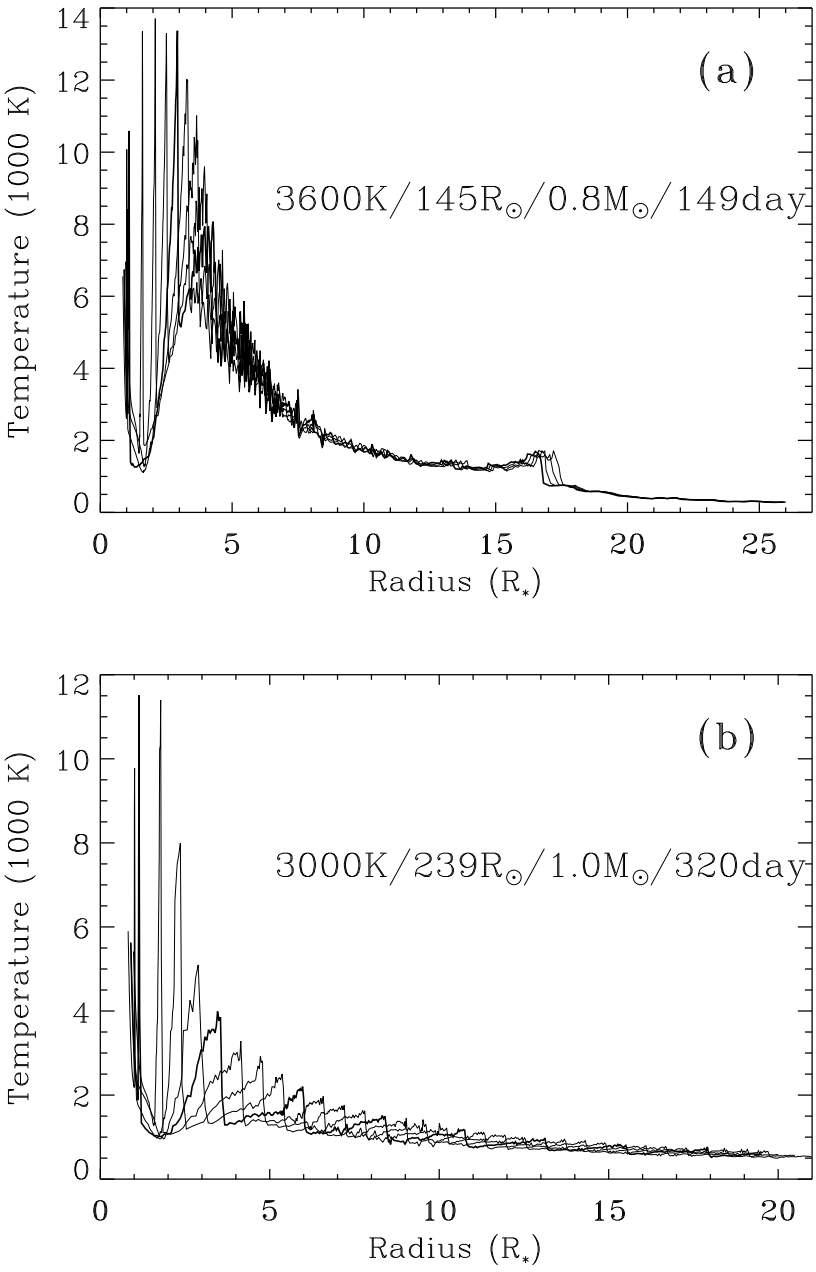

Figure 3. Two hydrodynamic models representative of Mira variables generated by Bowen (1988). Note that the model in (a) has no dust opacity whereas the model in (b) does have dust opacity included.

1.3. LTE versus non-LTE (NLTE) Radiative Transfer

The solution to the radiative transfer equation is typically handled by two approaches. The first is the assumption of local thermodynamic equilibrium (LTE), where the source function, S_ν, is set equal to the Planck function, $B_\nu(T)$. The actual definition of the source function is the ratio of the emissivity, η_ν, of a layer of gas to the total opacity, χ_ν, in that layer, hence $S_\nu \equiv \eta_\nu/\chi_\nu$. The total opacity is given by the sum of the absorption opacity and the scattering opacity. LTE also assumes the level and ion densities are determined through the Boltzmann and Saha equilibrium equations. The second approach, non-LTE (NLTE), solves the radiative transfer and net rate equations outright in a self-consistent manner (see Mihalas & Hummer 1973 for details).

Ideally, one should solve the transfer and rate equations in hydrodynamic calculations for LPV stars in order to determine the actual radiative cooling (and/or heating). Molecule and dust formation should be handled in a detailed manner and included in the above calculations. In practice this is difficult due to non-linearity of the equations and the large number of atmospheric zones and frequency points needed to carry out the calculations.

2. Modeling History

Initially, modelers of RGB and AGB stars ignored the Mira variables and instead concentrated on non-varying giants or the semiregular variables. These modelers typically assumed HSE and LTE in a time-independent, plane-parallel atmosphere (see Auman 1969; Alexander & Johnson 1972; Johnson 1973; Querci et al. 1974; Gustafsson et al. 1975; Tsuji 1976). One of most difficult aspects of stellar atmosphere modeling for cool stars is the inclusion of the millions of atomic and molecular bound-bound transitions. There are three basic techniques to include line opacity in atmospheric models: (1) *Mean Opacities*: Line opacity in a given frequency band is represented by a single number based upon approximated moments of the radiation field; (2) *Opacity Distribution Functions*: Line opacity in a given frequency band is represented by a function of temperature and density (or pressure) and sometimes velocity of the gas flow; and (3) *Opacity Sampling*: Line opacity calculated from all species within a given frequency width at a point in the spectrum for each atmospheric depth. Synthetic spectrum calculations of model atmospheres typically use the opacity sampling technique.

More recent HSE/RE (i.e., photospheric) models have dropped the plane parallel approximation in favor of spherical symmetry (see Brown et al. 1989; Plez et al. 1992). The first semiempirical (chromospheric) models of AGB stars (based on IUE spectra) were determined for the carbon star TX Psc (N0 II, SRc) (Luttermoser et al. 1989) and the oxygen-rich star g Her (M6 III, SRb) (Luttermoser et al. 1994) (see Figures 1 and 2). These chromospheric models retain the HSE approximation but drop the RE approximation.

Dynamic modeling of LPVs got its start in the 1970s. LPV modeling of Keeley (1970a) and Keeley (1970b) showed that the κ-mechanism from a hydrogen-ionization zone just beneath the photosphere could produce pulsations and account for the variability seen in these stars. Models by Wood (1974) suggested that Miras pulsate in the first-overtone mode from comparison of model veloc-

ities to observed values. Wood (1979) improved his dynamic models to allow either isothermal or adiabatic shocks to form. In the isothermal case, no continuous mass-loss is produced. In the adiabatic case, mass-loss is produced, but the gas-flow velocities do not match observations. Meanwhile, Hill & Willson (1979) and Willson & Hill (1979) used the isothermal approximation to determine that Miras pulsate in the fundamental mode.

Over the past few decades, dynamic modeling of LPVs has made significant improvements. Some of these improvements include the use of expressions to estimate radiative cooling in place of the isothermal and adiabatic approximations (e.g., Bowen 1988) and the inclusion of grain formation (e.g., Fleischer et al. 1992; Höfner et al. 1995). The Bowen (1988) hydrodynamic calculations found that non-dusty models generate an extended region of enhanced temperature from $\sim$2 to $\sim$8 $R_\star$ throughout the entire pulsation cycle (see Figure 3a). This enhanced temperature region above the photosphere resembles a *classical* chromosphere (i.e., $T_{\rm eff} \lesssim T \lesssim 10^4$ K) of static models and has been called a *calorisphere* by Willson & Bowen (1986), as well as, a *hydrodynamic chromosphere* by Dupree et al. (1990). Dusty models, on the other hand, present no such calorisphere.

However during this time period, others had still been using the isothermal shock approximation (e.g., Bessel et al. 1989). This approximation produces realistic velocities and mass loss in these models, as well as infrared synthetic spectra that are consistent with observed spectra. However, this approximation produces shocks with no temperature reversals. As such, no emission lines can be produced from such models. The ultraviolet (UV) and optical spectra of these stars show strong emission lines, and as such, the isothermal approximation cannot possibly be valid for the shocks in these stars. Also, since the observed emission lines are likely produced in the shocks, the adiabatic approximation must be invalid too since these lines will act as a coolant.

Radiative hydrodynamics is the only technique capable of producing realistic atmospheric models of these pulsating stars. The first attempts at detailed radiative hydrodynamic calculations for these stars began in the 1990s (e.g., Höfner et al. 1995; 2003). One problem with the Bowen (1988) hydrodynamics models of Miras is the thickness of the outward propagating shocks. The innermost shock of these models is optically thick in the hydrogen Balmer and Paschen continuum throughout much of the pulsation cycle which effects the emergent spectrum at optical and infrared wavelengths (see Luttermoser & Bowen 1992). Radiative hydrodynamic models of LPVs seemed to have solved this problem. Figure 3 of Höfner et al. (1995) displays such LPV models with thinner shocks (in temperature) as compared to the Bowen (1988) models. The shocks of these models will likely have optically thin hydrogen continua throughout the entire pulsation cycle which will produce more realistic synthetic spectra.

3. Observational Constraints

Optical brightness phase 0 in a Mira variable is defined as the time of maximum visual brightness. Spectroscopically these stars change a few subtypes in spectral class during light cycle. Strong emission lines from H-Balmer are seen, peaking in flux near phase 0 and disappearing around phase 0.6-0.7. Emission lines

from neutral iron appear around phase 0.2 at optical wavelengths. At early phases, the Hα emission line is weaker than the Hβ line, which in turn is weaker than the Hγ line, with Hδ being the strongest of the Balmer lines opposite to their line strengths (Gillet 1988). This observational effect is known as the *Balmer-line increment* and has been attributed to overlying obscuration due to molecular absorption (primarily from TiO). Before disappearing around phase 0.6, the strength of these lines resume their laboratory sequence of brightness (i.e., $f(\mathrm{H}\alpha) > f(\mathrm{H}\beta) > f(\mathrm{H}\gamma)$). This leads to some difficulty in the molecular absorption statement above since the TiO lines are still present in the spectra of these stars at these phases.

Meanwhile at ultraviolet wavelengths, the UV emission lines (dominated by Mg II) are not seem at phase 0 when the optical H-Balmer lines are at their brightest. Mg II begins to appear around phase 0.15 and peak in brightness near phase 0.3-0.4 then disappear around phase 0.7-0.8 (see Luttermoser 2000 and the references therein). This phase variability matches the phase variability of the neutral Fe lines which is expected since the Fe I lines are fluoresced by the Mg II lines. As such, there is an approximate 0.3 phase shift between the peak Balmer-line flux and the peak Mg II flux.

Any dynamic model constructed for these stars should obey the following observational characteristics:

- Produce macroscopic gas velocities that are consistent with the velocity measurements of certain spectral features (e.g., Mg II and Fe II lines).
- Produce observed mass-loss rates.
- Produce synthetic spectra that are consistent with the observed spectra of these stars including the UV and optical emission lines.

4. Synthetic Spectra of Mira Variable Stars

Luttermoser (1992); Luttermoser & Bowen (1992); Luttermoser (1996) has carried out a series of NLTE synthetic spectra calculations of some of the Bowen (1988) models. For these NLTE calculations, eight equally spaced pulsational phases were selected from the hydrodynamic model representing a *snapshot* approximation to the radiative transfer equation. For the calculations presented below, a 5-level model atom was used for hydrogen and a 6-level model was used for ionized magnesium. Though the Bowen models do have some problems with fitting the IR flux of Miras, these NLTE calculations have come up with new explanations for some of the spectral characteristics of these stars. Three important results were found from these calculations:

- The Balmer-lines vary in brightness in a manner similar to what is observed. Figure 4 shows profiles that were generated from initial *static*, plane-parallel calculations of the Bowen (1988) model shown in Figure 3a. These lines were calculated with background bound-bound opacities excluded to demonstrate the intrinsic changes of the Balmer lines without any effects of overlying absorption, sphericity, or gas velocity that could modify the line profile. Note that the peak flux in Hγ occurs near pulsational phase 0 and disappears near phase 0.5 similar to observed spectra.

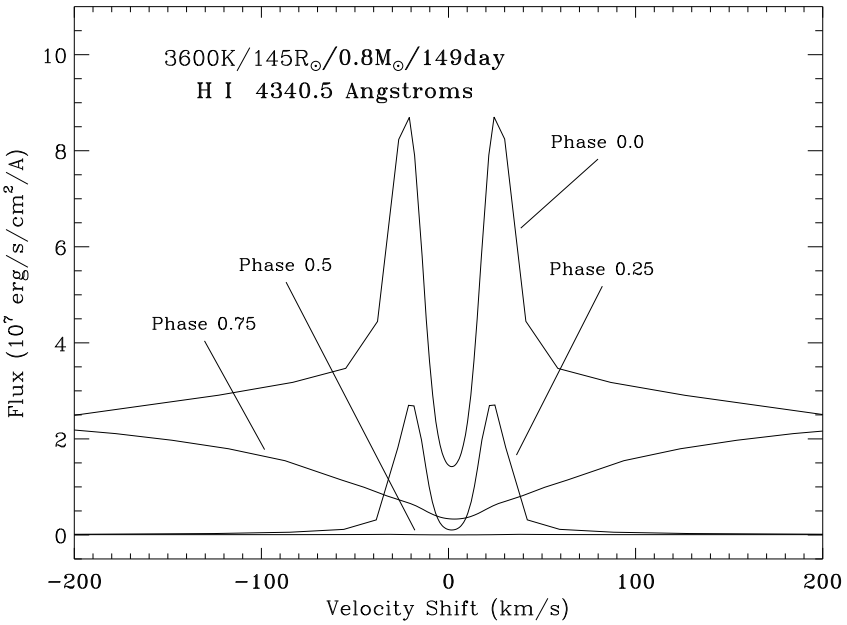

Figure 4. NLTE synthetic Hγ profiles for the 3600 K hydrodynamic model shown in Figure 3a at pulsational phases 0, 0.25, 0.5, and 0.75. The fluxes correspond to values at the stellar surface.

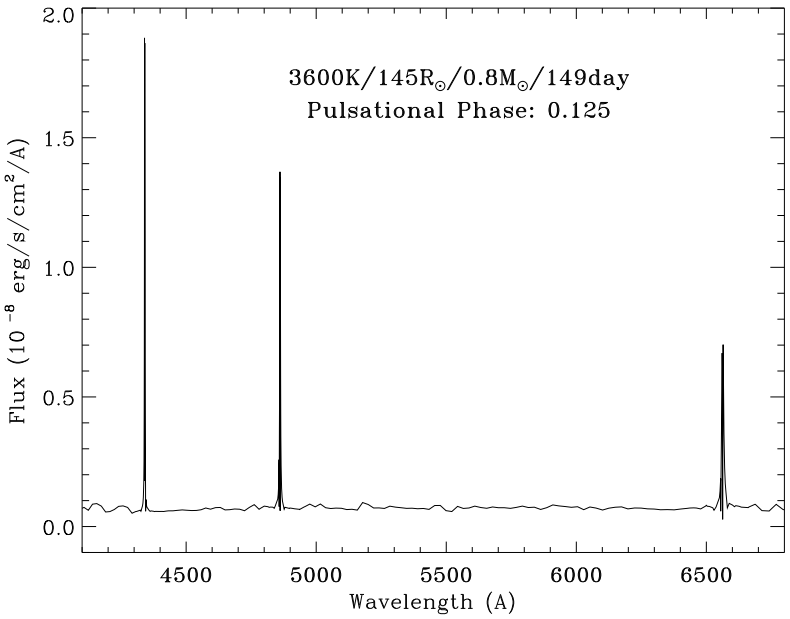

Figure 5. NLTE synthetic spectra at pulsational phase 0.125 from the Bowen model of Figure 3a. Note that the Balmer-line increment is clearly seen.

- The Balmer-line increment is produced (see Figure 5) without need of overlying absorption – it is a result of radiative transfer in the innermost shock. At later phases, the H synthetic spectra revert to a Balmer decrement as is observed.

- The Mg II lines are in absorption near phase 0 and do not reach maximum brightness until optical phase 0.3-0.4 which corresponds to observations.

The Balmer-line increment results from two factors in the transfer of radiation for the Balmer lines: (1) the optical depth (τ_ν) of the line which determines its depth of formation; and (2) the thermalization of the line which determines how closely the source function couples to the Planck function. Figure 6 demonstrates this phenomenon. The peak emission of these Balmer lines originates near *line-center* optical depth of 10^3 (note that the logarithm of the line-center optical depths, $\log \tau_\nu$, are located for each line within the plots of Figure 6). The core of the Hα line, which has the highest optical depth, forms in the 2nd innermost shock in the calorisphere near $\log \tau_\nu = 0$, while the emission wings originate in the temperature minimum region above the innermost shock at phase 0. Note that at this position in the atmosphere, S_ν(Hα), which is directly related to the number of photons being emitted in this line, is 4 orders of magnitude greater than the Planck function in this temperature minimum region, and is sloping downward from the values found in the innermost shock. Meanwhile, the Hβ emission feature forms in the post-shock region of the innermost shock. The higher gas temperature in this zone, as compared to the $\tau_\nu = 10^3$ zone of Hα, increases the collisional rates which causes S_ν(Hβ) to be more closely coupled to B_ν. Since S_ν(Hβ) $> S_\nu$(Hα) near $\tau_\nu = 10^3$ for each line, the flux of Hβ is greater than Hα. Hγ, with its even lower oscillator strength, 'sees' a little deeper in the innermost shock, hence samples an even hotter part of the post-shock region. The resulting Hγ emission line is stronger than the Hβ line. By extrapolation of this 5-level atomic model, the Hδ line must sample the hottest part of the innermost shock and the higher order Balmer lines have optical depths low enough that they start to 'see' through the innermost shock and weaken as compared to Hδ matching the observed characteristics of the Balmer series in Miras.

As the innermost shock continues to propagate outward, it begins to merge into the calorisphere around pulsational phase 0.375. At this point, the Balmer-line emission originate in the calorisphere and take on the more standard 'chromospheric' appearance (i.e., f(Hα) $> f$(Hβ) $> f$(Hγ)), which agrees with the observations. The lines weaken and vanish shortly thereafter. They reappear around pulsational phase 0.875 when the next strong shocks arises out of the photosphere. This cycle seen in the synthetic spectra mimics the observed variability very well.

Typically, around phase 0.2, emission lines from neutral metals (see Figure 7), particularly Fe I, begin to appear in the blue at optical wavelengths and these reach a peak flux around phase 0.3-0.4 as the star pulsates. At UV wavelengths (as observed with IUE), emission lines do not appear until phase 0.15 where they continue to gain strength in time until reaching a maximum around phase 0.3-0.4, similar to the neutral metal lines. This 0.3-0.4 phase shift between the peak Mg II flux and Balmer-line flux is due to the fact that the Mg II lines form in the calorisphere throughout the entire pulsation cycle and not in

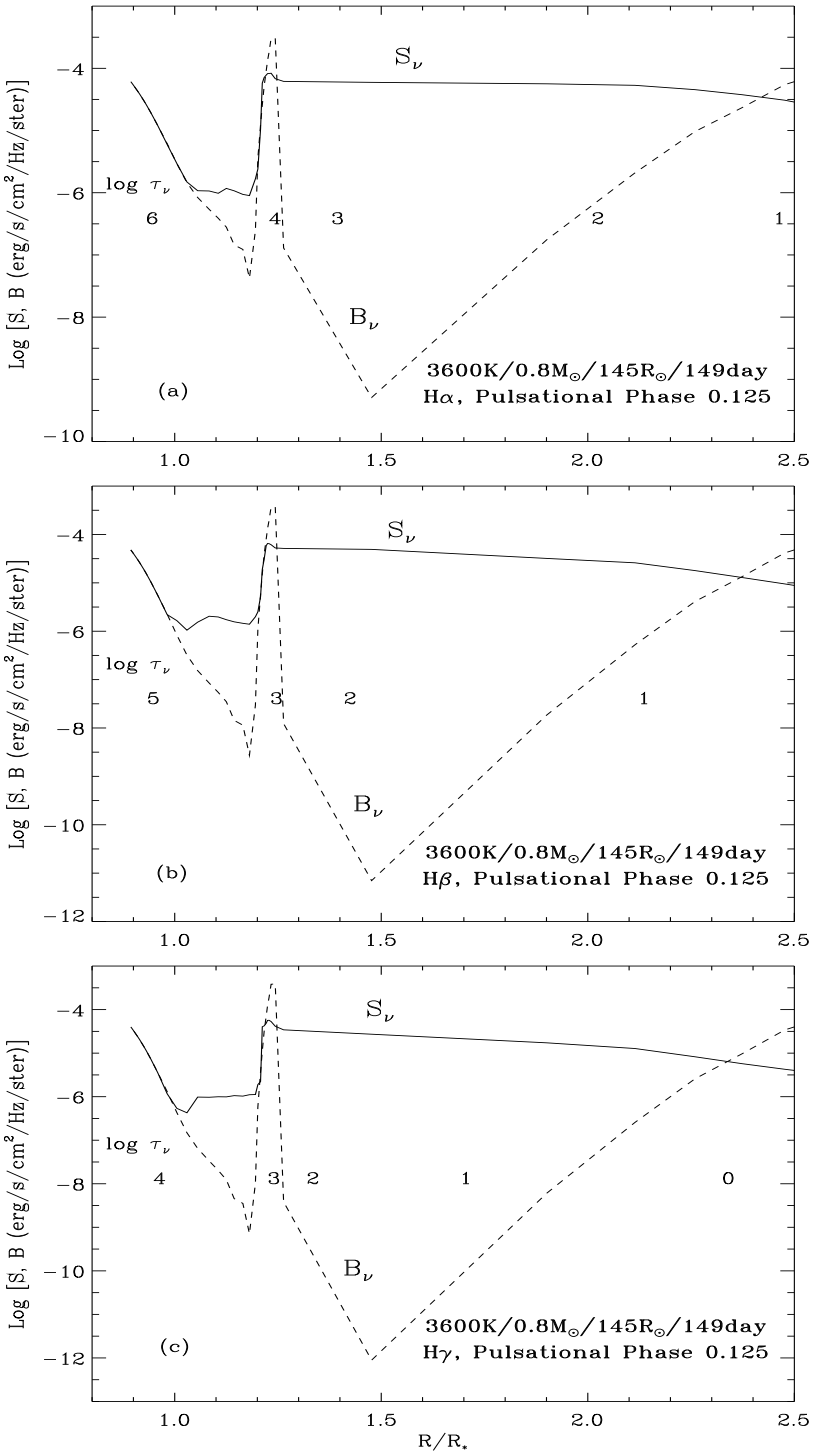

Figure 6. The Balmer-line source and Planck functions for the profiles shown in Figure 5: (a) Hα, (b) Hβ, and (c) Hγ. Note that the peak emission in these lines arises from *line-center* optical depth near 10^3.

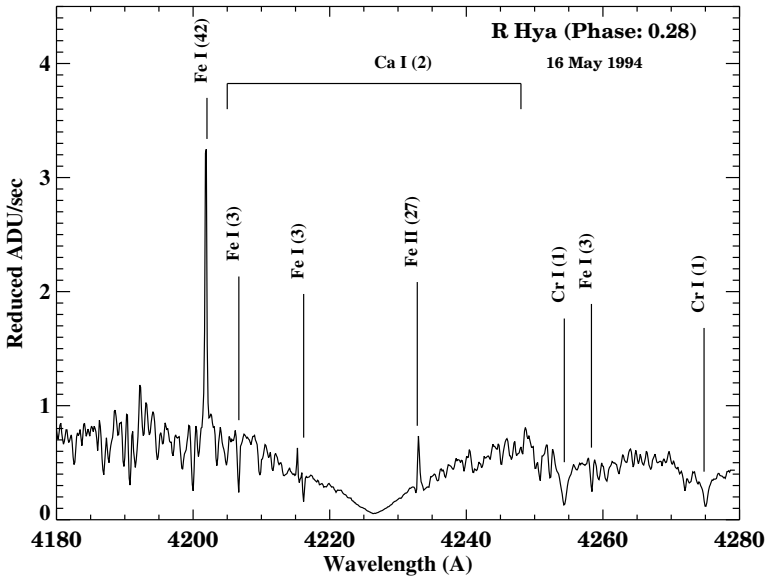

Figure 7. Observed spectra in the Ca I (optical multiplet 2) resonant line region at visual light phase 0.28 for the Mira variable R Hya. Note the strong Fe I (42) lines at 4202 Å which is fluoresced by the Mg II k line at 2795.5 Å. This spectrum was obtained with the McMath-Pierce telescope on Kitt Peak on 16 May 1994.

the innermost shock unlike the Balmer lines. Hence, the UV peak emission phase shift from the Balmer lines results from the existence of a permanent hydrodynamic chromosphere.

Figure 8 shows a series of high-dispersion IUE spectra of R Leo in the Mg II h & k region. Most non-Mira red giant stars display *effectively-thin* Mg II h & k lines (e.g., Judge et al. 1993) – lines that show double-lobed emission features with an integrated flux ratio of $F(\mathrm{k})/F(\mathrm{h}) \approx 1.5$, the ratio of their respective oscillator strengths. IUE observations have shown us that this is not the case for Miras. When Mg II is near its peak flux ($\sim$ phase 0.3-0.4), $F(\mathrm{k}) < F(\mathrm{h})$, then slowly take on the more normal, effectively-thin $F(\mathrm{k})/F(\mathrm{h}) > 1$ as the flux of these lines fade past phase 0.5. These IUE spectra (and later HST spectra) give a strong indication that the relative weakness of the k line with respect to the h line results from absorption from Fe I and Mn I in a cooler overlying shell. Another obvious feature of the Mg II doublet is the large blue shift of the emission of these lines with respect to the rest velocity of the star (as shown by dashed lines in Figure 8). Such blue shifts are not seen in the non-Mira red giants and the cause of this shift is still debated (see Luttermoser 2000 for further details of the UV emission lines in Miras).

5. Where Do We Go From Here?

As seen by this review, atmospheric modeling of Mira variable stars is very complicated and difficult. Non-equilibrium processes are present in the radiative

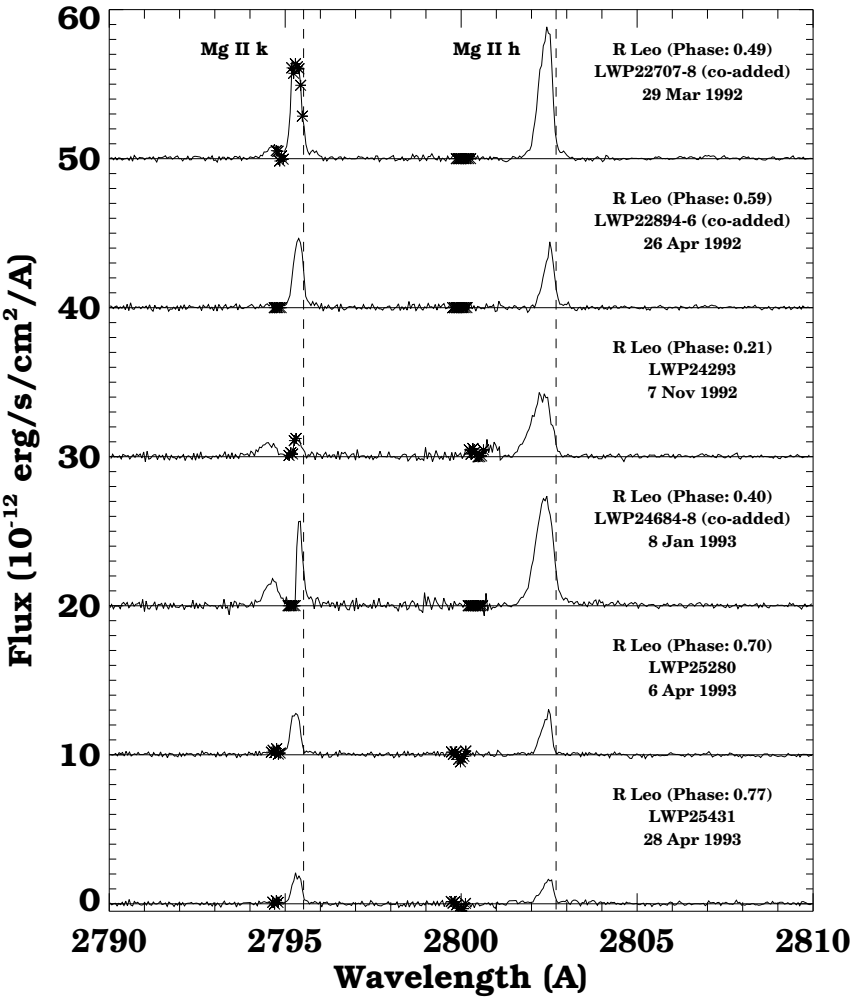

Figure 8. A series of high-dispersion IUE spectra of R Leo in the Mg II k & h region taken at various phases over two pulsation cycles from Luttermoser (2000). Reseau marks and saturated pixels are marked with '$*$'. All spectra have been shifted by -7.2 km/s to offset the center-of-mass velocity of R Leo. The laboratory wavelengths of Mg II h & k are indicated with a vertical dashed line.

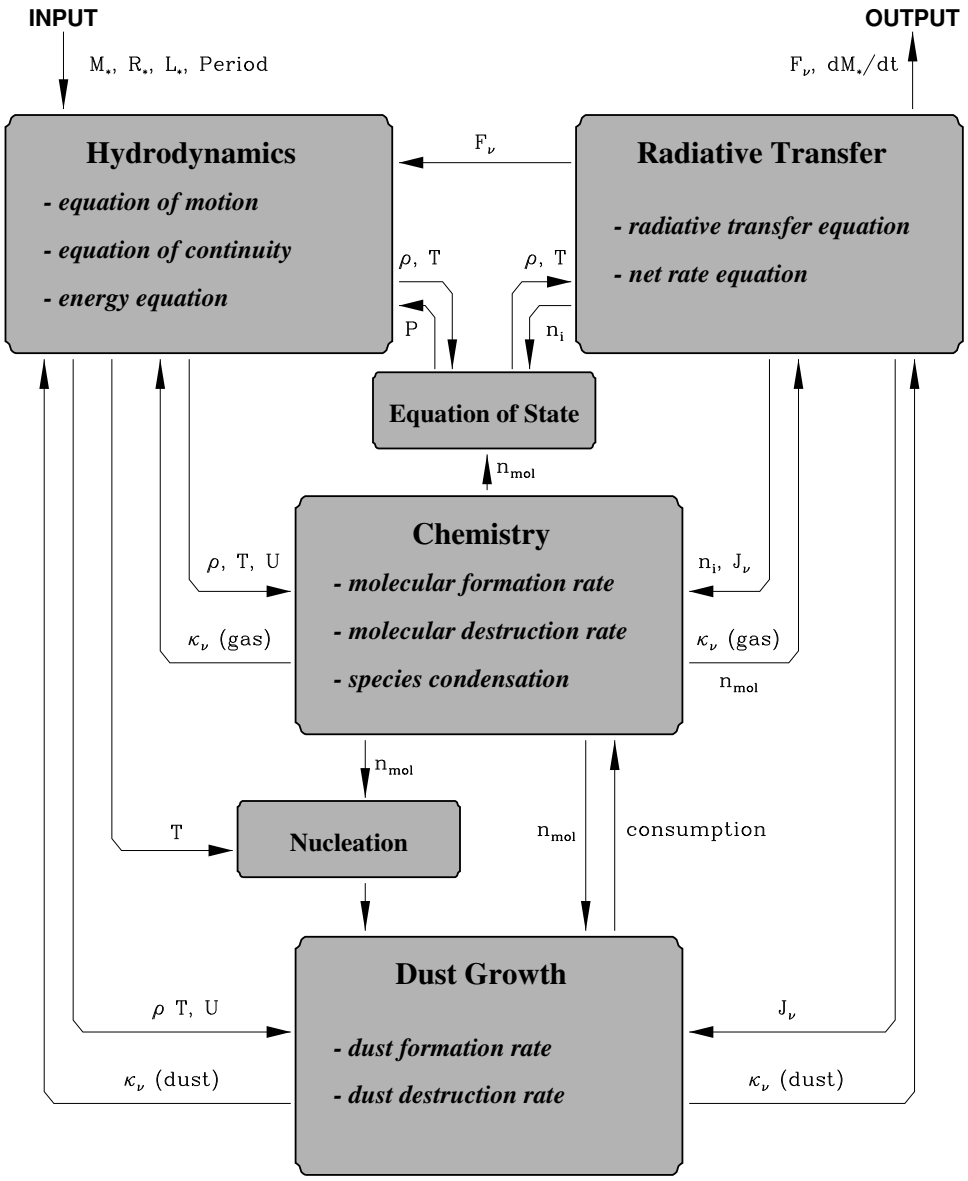

Figure 9. A schematic showing the complexities and interdependencies of various physical processes required for the modeling of cool variable stars in a self-consistent manner. This diagram was inspired by Figure 4 of Sedlmayr (1994).

processes, excitation, ionization, chemistry, and dust formation in these dynamic atmospheres as summarized by Figure 9. In addition to the non-equilibrium processes that should to be included, other questions need to be addressed in future modeling:

- Do spatial inhomogeneities exist across the surface of these stars?
- Are there radial inhomogeneities in composition?
- Are surface magnetic fields present, and if so, are they local and/or global?

Convection has typically been included in the modeling of these stars via the mixing-length theory. However, to make the most accurate models of these pulsating stars, 3-dimensional convection calculations should be used as demonstrated by Jacobs et al. (2001) and Frytag (2006). Finally, in addition to addressing all of the items mentioned above, 3-dimensional NLTE radiative hydrodynamics should be investigated as well. Unfortunately, carrying out all of these computationally difficult processes will likely have to wait for computers to get a few orders of magnitude bigger in RAM and storage space and a few orders of magnitude faster in speed.

Acknowledgments. A special thanks is made to the following people who have been important to my research concerning Mira variable stars: Hollis Johnson, Gene Avrett, Rudy Loeser, Robert Stencel, and especially Lee Anne Willson and George Bowen. Much of my work reported here was supported by the following research grants and contracts from NASA: NAG 5-1181, NAG 5-1305, NAG 5-1777, and NAS 5-32863. Finally, I am grateful for the observing assistance from the staff at the IUE Observatory at NASA/Goddard Space Flight Center and the staff of the National Solar Observatory at Kitt Peak, Arizona during the years my observational data were obtained.

References

Alexander, D.R. & Johnson, H.R. 1972, ApJ, 176, 629
Auman, J.R. 1969, ApJ, 157, 799
Bessell, M. S., Brett, J. M., Wood, P. R., & Scholz, M. 1989, A&A, 213, 209
Bowen, G.H. 1988, ApJ, 329, 299
Brown, J.A., Johnson, H.R., Alexander, D.R., Cutright, & L., Sharp, C.M. 1989, ApJS, 71, 623
Dupree, A.K., Hartmann, L., & Smith, G.H. 1990, in Sixth Cambridge Workshop on Cool Stars, Stellar Systems, and the Sun, ed. G. Wallerstein, A.S.P. Conference Series, 9, 408
Fleischer, A. J., Gauger, A., & Sedlmayr, E. 1992, A&A, 266, 321
Frytag, B. 2006, in Stellar Fluid Dynamics and Num. Simulations: From the Sun to Neutron Stars, ed. M. Rieutord & B. Dubrulle, EAS Publications Series, 21, 325
Gillet, D. 1988, A&A, 192, 206
Gustafsson, B., Bell, R. A., Eriksson, K., & Nordlund, A. 1975, A&A, 42, 407
Hill, S.J. & Willson, L.A. 1979, ApJ, 229, 1029
Höfner, S., Feuchtinger, M. U., & Dorfi, E. A., A&A, 297, 815
Höfner, S., Gautschy-Loidl, R., Aringer, B., & Jrgensen, U. G. 2003, A&A, 399, 589
Jacobs, M.L., Porter, D.H., Merkey, B.V., & Woodward, P.R. 2000, BAAS, 32, 1426
Johnson, H.R. 1973, ApJ, 180, 81

Judge, P.G., Luttermoser, D.G., Neff, D.H., Cuntz, M., & Stencel, R.E. 1993, AJ, 105, 1973
Keeley, D.A. 1970, ApJ, 161, 643
Keeley, D.A. 1970, ApJ, 161, 657
Luttermoser, D.G. 1992, in 7th Cambridge Workshop on Cool Stars, Stellar Systems, and the Sun, ed. M.S. Giampapa & J.A. Bookbinder, ASP Conf. Series, 26, 506
Luttermoser, D.G. 1996, in 9th Cambridge Workshop on Cool Stars, Stellar Systems, and the Sun, ed. R. Pallavicini & A.K. Dupree, ASP Conf. Series, 109, 535
Luttermoser, D.G. 2000, ApJ, 536, 923
Luttermoser, D.G. & Bowen, G.H. 1992, in 7th Cambridge Workshop on Cool Stars, Stellar Systems, and the Sun, ed. M.S. Giampapa & J.A. Bookbinder, ASP Conf. Series, 26, 558
Luttermoser, D.G., Johnson, H.R., Avrett, E.H, & Loeser, R. 1989, ApJ, 345, 543
Luttermoser, D.G., Johnson, H.R., & Eaton, J.A. 1994, ApJ, 422, 351
Mihalas, D. & Hummer, D.G. 1973, ApJS, 28, 343
Plez, B., Brett, J.M., & Nordlund, A. 1992, A&A, 256, 551
Querci, F., Querci, M., & Tsuji, T. 1974, A&A, 31, 265
Sedlmayr, E. 1994, in Molecules in the Stellar Environment, ed. U.G. Jørgensen, Berlin: Springer-Verlag, 163
Tsuji, T. 1976, Publ. Astron. Soc. Japan, 28, 543
Willson, L.A. & Bowen, G.H. 1986, in Fourth Cambridge Workshop on Cool Stars, Stellar Systems, and the Sun, ed. M. Zeilik & D.M. Gibson, (Springer–Verlag: Berlin), 385
Willson, L.A. & Hill. S.J. 1979, ApJ, 228, 854
Wood, P.R. 1974, ApJ, 190, 609
Wood, P.R. 1979, ApJ, 227, 220